AIAA JOURNAL
Vol. 41, No. 12, December 2003

Deformation and Drag Properties of Round Drops Subjected to Shock-Wave Disturbances

C. Aalburg,* B. van Leer,† and G. M. Faeth‡
University of Michigan, Ann Arbor, Michigan 48109-2140

The deformation, drag, and breakup properties of round drops subjected to shock-wave disturbances were studied computationally for conditions where effects of drop evaporation were small. The objective of the study was to consider effects of liquid viscosity, liquid/gas density ratio, and drop Reynolds number that are difficult to explore based on experiments but are representative of conditions found in practical sprays. The time-dependent incompressible and axisymmetric Navier–Stokes equations were solved in both the gas and liquid phases in conjunction with the level set method to determine the position of the liquid/gas interface for deforming drops. The numerical results were evaluated using earlier experimental results for the wake and drag properties of solid spheres and the deformation and drag and breakup properties of drops subjected to shock-wave disturbances. There was good agreement between measurements and predictions. The properties of drop deformation and breakup were mainly affected by the drop drag-force/surface-tension-force ratio represented by the Weber number *We* and the drop liquid-viscous-force/surface-tension-force ratio represented by the Ohnesorge number *Oh*. When the *Oh* was small, drop deformation and breakup transitions yielded the classical deformation and breakup regime map suggested by Hinze roughly 50 years ago. However, when the *Oh* was large the computations revealed undesirable variations of *We* as a function of *Oh* for particular deformation and breakup regime transitions when plotted in the classical Hinze form. An improved approach to handle large *Oh* conditions was found, however, by directly plotting the drop drag-force/liquid-viscous-force ratio $We^{1/2}/Oh$, as a function of the drop surface-tension-force/liquid viscous-force ratio $1/Oh$ because $We^{1/2}/Oh$ is relatively independent of *Oh* at the regime transitions when the *Oh* is large. Effects of liquid/gas viscosity and density ratios on the new deformation and breakup regime map were found to be small. The Reynolds number of the gas flow over the drop, however, was found to have a considerable effect on drop deformation and breakup properties as the low Reynolds number (<100), Stokes flow, regime was approached. This behavior appears to be caused by the progressive increase of the drop drag coefficient when the Reynolds number of the gas flow becomes small, which tends to reduce drop relaxation times and thus times available for drop deformation and breakup.

Nomenclature

C_D	=	drag coefficient
d	=	drop diameter
L	=	wake length
n_r	=	unit normal vector in the radial direction
n_x	=	unit normal vector in the streamwise direction
Oh	=	initial Ohnesorge number, $\mu_L/(\rho_L\sigma d_0)^{1/2}$
p	=	pressure
Re	=	initial Reynolds number, $\rho_G u_0 d_0/\mu_G$
r	=	radial distance
t	=	time
t^*	=	characteristic breakup time, $d_0(\rho_L/\rho_G)^{1/2}/u_0$
u	=	streamwise velocity
v	=	radial velocity
We	=	initial Weber number, $\rho_G u_0^2 d_0/\sigma$
x	=	streamwise distance
δ	=	unit delta function
κ	=	curvature
μ	=	molecular viscosity
ρ	=	density
σ	=	surface tension

Subscripts

c	=	maximum cross-stream dimension
cr	=	critical value
G	=	gas phase property
L	=	liquid phase property
max	=	maximum value
min	=	minimum value
0	=	initial condition

Received 4 November 2002; revision received 23 June 2003; accepted for publication 2 July 2003.

*Research Fellow, Department of Aerospace Engineering.
†Professor, Department of Aerospace Engineering. Fellow AIAA.
‡A. B. Modine Professor, Department of Aerospace Engineering. Fellow AIAA.

Introduction

STUDY of the deformation and drag properties of round drops subjected to shock-wave disturbances is motivated by applications to the secondary breakup of drops within sprays found in power, propulsion, and combustion systems. In particular, the time required for the shock wave itself to transit the drop is too small for significant drop response to this direct interaction. Instead, the drop passes into the uniform flowfield behind the shock wave, approximating a step change of the flow around the drop, typical of disturbances leading to secondary drop breakup upon the completion of primary drop breakup in practical sprays. The present study is an extension of several past experimental studies of secondary drop breakup, for conditions where effects of drop evaporation are small, in this laboratory.[1–6] These earlier studies found that deformation and breakup regime transitions were mainly affected by the Weber number We as a measure of the drop drag-force/surface-tension-force ratio and the Ohnesorge number Oh as a measure of the drop liquid-viscous-force/surface-tension-force ratio, as proposed by Hinze[7] roughly 50 years ago. Because of experimental constraints, however, drop deformation and breakup measurements generally are limited to large liquid/gas density ratios $\rho_L/\rho_G = 580$–12,000, intermediate Reynolds numbers for the initial gas flow over the drop $Re = 3 \times 10^2$–16×10^3, and a relatively narrow range of

liquid viscosities and liquid/gas viscosity ratios, and deformation and breakup behavior for other property conditions are unknown.

The objective of the present investigation was to consider effects of liquid and gas properties on drop deformation and drag properties, using numerical simulations in order to explore property variations that are difficult to consider with experiments. The present study could not consider drop breakup directly, however, because breakup is a complex, three-dimensional process, because of the formation of nodes, that would require locally very fine three-dimensional grids that are not computationally tractable for parametrically extensive temporal calculations of deforming bodies at the present time. Experimental observations of secondary drop breakup caused by shock-wave disturbances from Hsiang and Faeth,[3] Chou et al.,[5] and Dai and Faeth,[6] however, have shown that the onset of secondary breakup can be associated with drop deformations of 70–100%, and the results of the present predictions, to be discussed later, support this conclusion as well. Thus, by adopting this finding, it was possible to estimate conditions for the onset of secondary drop breakup without having to calculate the details of the breakup process itself, pending the future feasibility of more definitive time-dependent three-dimensional numerical simulations of drop breakup for large parameter ranges similar to those considered during the present study. As a result, present numerical calculations were axisymmetric and reasonably tractable, allowing extensive parametric study of a number of drop breakup properties.

Representative earlier studies that sought to use numerical simulations to study the properties of secondary breakup include Zaleski et al.[8] and Han and Tryggvason.[9,10] Zaleski et al.[8] consider the secondary breakup of cylindrical liquid elements subjected to a step change of the ambient velocity in crossflow (which is equivalent to a shock-wave disturbance); these results were limited to a liquid/gas density ratio of 10 and really are more appropriate for a simulation of the breakup of a nonturbulent round liquid jet in a uniform crossflow than for a simulation of the secondary breakup of drops subject to a shock-wave disturbance. Han and Tryggvason[9,10] considered the secondary breakup of round drops for liquid/gas density ratios of 1.15 and 10.0, treating effects of step changes of ambient velocity and acceleration. Thus, the main focus of the present numerical simulation effort was to consider a broader range of liquid/gas density ratios (2–∞), which allowed evaluation of the predictions using available measurements in the literature and provided new information about effects of drop liquid and gas properties on the deformation and breakup of drops.

The present calculations were evaluated based on earlier results for a variety of properties of flow over spheres and drop deformation, as follows: wake sizes and drag coefficients of solid spheres, the properties of steady drop deformation in the presence of a constant body force, and the extent of deformation and conditions at the onset of breakup caused by shock-wave disturbances. Numerical simulations were then carried out for a range of parameters to study effects of Weber number ($We = 0.25$–10^9), Ohnesorge number ($Oh = 0.001$–10^3), Reynolds number ($Re = 10$–10^3), liquid/gas density ratio ($\rho_L/\rho_G = 2$–∞), and liquid/gas viscosity ratio ($\mu_L/\mu_G = 0.02$–13,000), on the deformation, drag, and breakup properties of liquid drops subjected to step changes of flow properties (typically approximated by shock-wave disturbances during experimental investigations).

Numerical Computations

Computational Methods

The time-dependent incompressible axisymmetric Navier–Stokes equations, in the following conservative form:

$$\frac{\partial u}{\partial x} + \frac{\partial v}{\partial r} + \frac{v}{r} = 0 \tag{1}$$

$$\frac{\partial(\rho u)}{\partial t} + \frac{\partial(\rho u^2)}{\partial x} + \frac{1}{r}\frac{\partial(r\rho uv)}{\partial r} = -\frac{\partial p}{\partial x} + \frac{\partial}{\partial x}\left(2\mu\frac{\partial u}{\partial x}\right) + \frac{1}{r}\frac{\partial}{\partial r}\left(r\mu\left[\frac{\partial v}{\partial x} + \frac{\partial u}{\partial r}\right]\right) + \delta\sigma\kappa n_x \tag{2}$$

$$\frac{\partial(\rho v)}{\partial t} + \frac{\partial(\rho uv)}{\partial x} + \frac{1}{r}\frac{\partial(r\rho v^2)}{\partial r} = -\frac{\partial p}{\partial r} + \frac{\partial}{\partial x}\left(\mu\left[\frac{\partial v}{\partial x} + \frac{\partial u}{\partial r}\right]\right) + \frac{\partial}{\partial r}\left(2\mu\frac{\partial v}{\partial r}\right) + 2\mu\frac{\partial}{\partial r}\left(\frac{v}{r}\right) + \delta\sigma\kappa n_r \tag{3}$$

were solved in both the gas and liquid phases using the projection method of Chorin[11] with a multigrid Poisson solver for the pressure equation. The discretization in space was carried out on a staggered grid according to the marker and cell (MAC) method of Harlow and Welch.[12] The level set method of Sussman et al.[13] was used to capture the liquid/gas interface, which yielded the local fluid properties of each cell with a smooth transition between the gas and the liquid phases near the interface. A redistancing algorithm according to Sussman and Fatemi[14] was used to maintain the level set as an accurate distance function at all times. The interface calculations allowed for effects of surface tension, pressure, and shear forces, with surface tension represented as a body force distributed over the interface having finite thickness, following Brackbill et al.[15] The discretizations in both space and time were second-order accurate.

The domain size was typically 7.5 $r_0 \times 15\,r_0$ and was covered with a moving grid having 192×384 cells. One side of the domain corresponded with the axis of symmetry of the drop. The boundary conditions were symmetric along the sides of the domain, with a fixed velocity across the inlet and a fixed pressure across the outlet. The streamwise distance traveled by the drops caused by the acceleration caused by the ambient flow could be quite considerable; therefore, a row of computational cells was deleted from the inlet and added to the outlet by extrapolating radial velocities whenever the center of mass crossed another grid row. As a result of this procedure, the center of mass of the drop was maintained roughly $\frac{1}{3}$ of the streamwise distance from the inlet of the computational domain. Tests with solution regimes of double size ($15\,r_0 \times 30\,r_0$) and finer grids (384×768 cells) caused less than a 3% change, at deformation conditions approaching breakup, from the results reported here. The simulations were started with an initially motionless radial plane of the drop being subjected to a sudden divergence-free velocity field. This condition is equivalent to the step change in the ambient velocity that a drop experiences immediately after the passage of a shock-wave disturbance during shock-tube experiments of secondary drop breakup. Except for consideration of drop deformation in the presence of constant body forces, effects of buoyancy were neglected. The flow was assumed to be isothermal with constant liquid- and gas-phase properties, with negligible effects of drop vaporization, which corresponds to the conditions of the measurements used to evaluate present computations.

Computational Evaluation

Prior to considering the deformation and breakup properties of deforming drops, the numerical computations were evaluated using earlier measurements and computations concerning the flow over stationary solid nondeforming spheres (solid spheres). This included both the steady wake lengths and the drag coefficients of solid spheres as a function of the Reynolds number of the flow over the spheres [limited to conditions prior to the transition to unsteady (oscillating) wakes at $Re = 130$].

Visualizations of the streamline pattern of the flow over solid spheres at Reynolds numbers, $Re = 20$, 40, 80, and 120, are illustrated in Fig. 1. The present computations provide the temporal variation of the flow; however, the time of the results shown in Fig. 1, $tu_0/d_0 = 15$, is sufficiently large for the streamline patterns to provide an accurate representation of steady streamline patterns. For the smallest Reynolds-number conditions illustrated in Fig. 1, $Re = 20$, the flow over the sphere reattaches smoothly at the downstream stagnation point of the sphere, and there is no recirculating wake region. Recirculating wakes are similarly absent for $Re < 20$, extending into the creeping flow, or Stokes flow regime. For $Re > 20$, however, a recirculating wake appears having an annular configuration with the length that the recirculating wake projects in the streamwise direction progressively increasing with increasing Reynolds numbers.

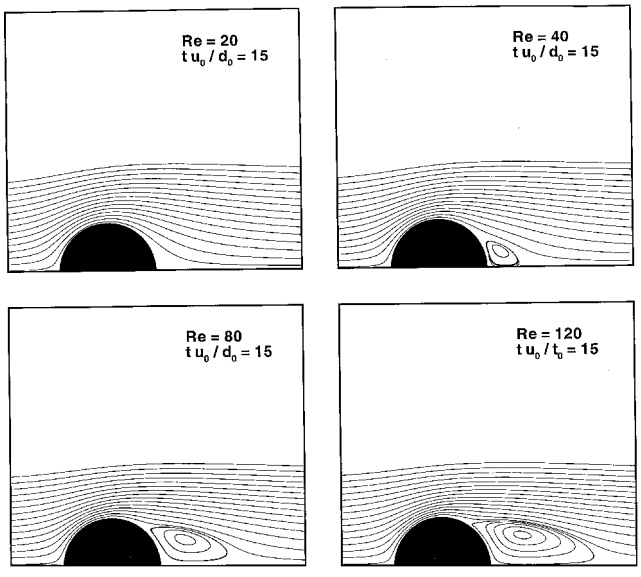

Fig. 1 Nearly steady streamlines around a solid sphere at Reynolds numbers of 20, 40, 80, and 120.

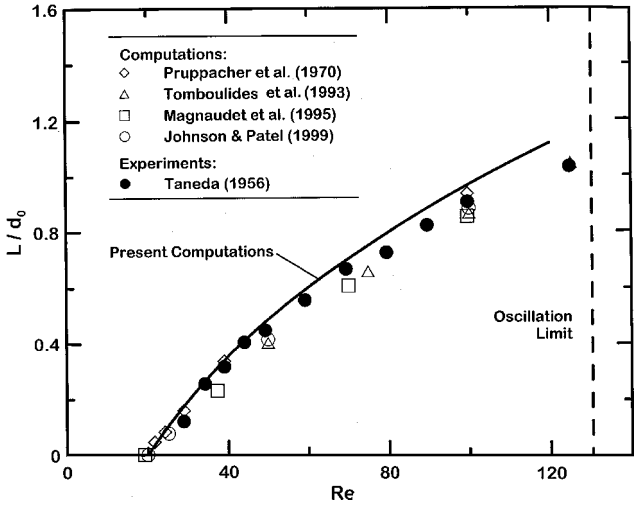

Fig. 2 Measured and predicted steady wake length behind a solid sphere as a function of Reynolds number for values smaller than the onset of instabilities ($Re < 130$). Measurements from Taneda,[16] predictions from Pruppacher et al.,[17] Tomboulides et al.,[18] Magnaudet et al.,[19] Johnson and Patel,[20] and the present investigation.

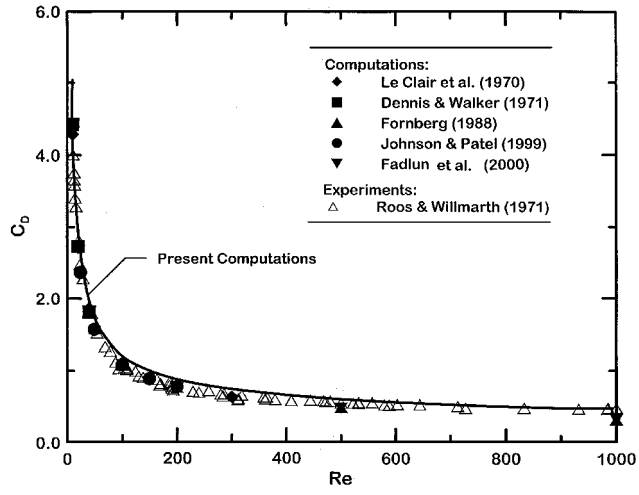

Fig. 3 Measured and predicted drag coefficients as a function of Reynolds number for solid spheres. Measurements from Roos and Willmarth,[21] predictions from Johnson and Patel,[20] LeClair et al.,[22] Dennis and Walker,[23] Fornberg,[24] Fadlun et al.,[25] and the present investigation.

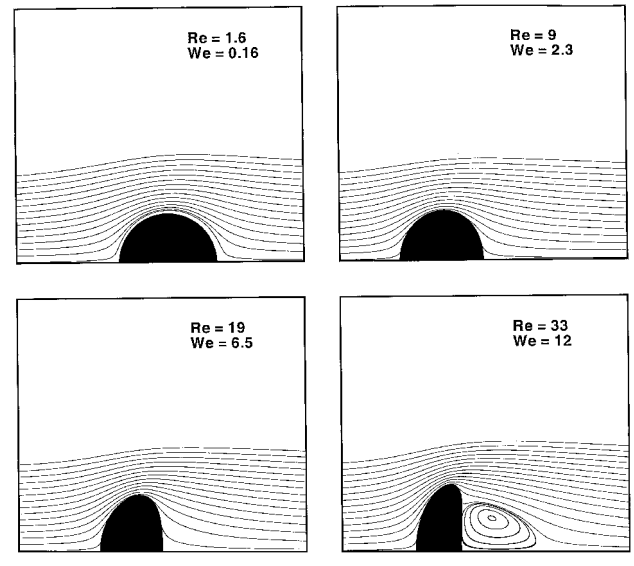

Fig. 4 Steady streamline patterns for the steady wakes behind deforming drops accelerated by constant body forces for Weber numbers of 0.16, 2.3, 6.5, and 12.

Present predictions of the recirculating wake length L, measured from the downstream stagnation point of the solid sphere to the point where the flow reattaches at the axis normalized by sphere diameter d_0, are plotted as a function of Reynolds number in Fig. 2. Also shown on the figure are earlier determinations of L/d_0 from the experiments of Taneda[16] and the numerical computations of Pruppacher et al.,[17] Tomboulides et al.,[18] Magnaudet et al.,[19] and Johnson and Patel.[20] All of the predictions are in good agreement with the measurements, correctly indicating first appearance of a recirculating wake at $Re = 20$ and the subsequent progressive increase of L/d_0 with increasing Reynolds number. The measurements show that the wakes become unsteady and begin to oscillate at $Re = 130$; the present steady and axisymmetric computations are no longer appropriate at such conditions, and predicted and measured values of L/d_0 are terminated at this condition.

The present predictions of the drag coefficients C_D of solid spheres, calculated from the momentum loss of the continuous phase as it flows over the sphere, are plotted as a function of Reynolds number for $Re = 10$–10^3 in Fig. 3. Also shown on the figure are earlier determinations of C_D from the experiments of Roos and Willmarth[21] and from the numerical computations of Johnson and Patel,[20] LeClair et al.,[22] Dennis and Walker,[23] Fornberg,[24] and Fadlun et al.[25] The agreement between the measurements and all of the predictions is excellent, showing that C_D is relatively constant for $Re > 100$ but increases dramatically as Reynolds number decreases toward the Stokes regime for $Re < 100$. Notably, the predictions of C_D remain quite good for $Re > 130$, in spite of the unsteadiness of the wakes at these conditions. This behavior suggests that the wake unsteadiness does not have a significant effect on solid sphere drag properties for these conditions.

Taken together, the results illustrated in Figs. 2 and 3 suggest that present numerical computations provide a reasonably good representation of the continuous phase flow over solid spheres. Evaluation of the computations will continue by considering drop deformation; these results are considered next.

Results and Discussion

Drop Deformation in Response to Steady Disturbances

The steady streamlines and shapes of drops being accelerated by a constant body force (gravity) are illustrated in Fig. 4. The predictions illustrated in this figure were completed for ethylene glycol

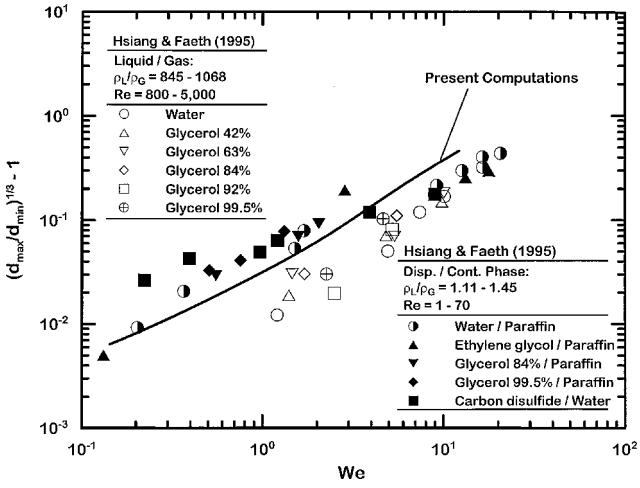

Fig. 5 Measured and predicted steady drop deformation caused by a constant body force as a function of Weber number. Measurements from Hsiang and Faeth[3] and predictions from the present investigation.

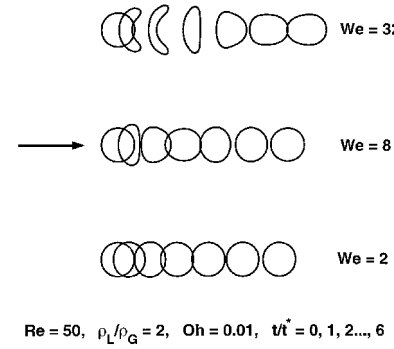

Fig. 6 Visualization of liquid drop cross sections as a function of time for various Weber numbers ($Re = 50, \rho_L/\rho_G = 2, Oh = 0.01$; time of images $t/t^* = 0, 1, 2, 3, 4, 5,$ and 6).

drops dispersed in paraffin oil at four different Weber numbers that were achieved by varying the diameters of the drops. The computed results are obtained at sufficiently large times so that unsteady effects were small and steady streamlines can be illustrated. For such conditions a variation of the Weber number causes a corresponding variation of the Reynolds number of the flow over the drop as indicated on the plot. Typical of steady drop deformation measurements in the literature, a progressive increase of the Weber number causes a corresponding progressive increase of the deformation of the drop. Notably, the appearance of a recirculating wake behind the deformed drop occurs near $Re = 30$, which is not very different from results considered earlier concerning flows around solid spheres, as discussed in connection with Figs. 1 and 2. The length of the wake behind a deformed drop, however, is larger than the length of a wake behind a solid sphere at comparable conditions (for example, compare Figs. 1 and 4), as a result of the effect of deformation modifying the location where the flow separates from the drop.

Predictions and measurements of the deformation of drops being accelerated by a constant body force (gravity) are illustrated in Fig. 5. The predictions illustrated in this figure were completed for ethylene glycol drops moving in paraffin oil, at terminal velocity conditions, similar to Fig. 4. Measured deformations for similar conditions reported by Hsiang and Faeth[3] are also illustrated on the plot. For these results deformation is represented by the parameter $(d_{\max}/d_{\min})^{1/3} - 1$, where $d_{\max}$ and $d_{\min}$ are the maximum (cross stream) and minimum (streamwise) dimensions of the drop. The measurements of Hsiang and Faeth[3] involve a variety of drop/continuous-phase systems having different liquid/gas density and viscosity ratios and Reynolds numbers (with Reynolds numbers in the range $1\text{–}5 \times 10^3$) at particular Weber number conditions. The wide range of drop/continuous-phase properties no doubt contributes to the scatter seen in Fig. 5; nevertheless, present predictions of drop deformation are in reasonable agreement with the measurements for the ethylene glycol drops in paraffin oil that were specifically considered. In particular, the rms differences between measurements and present predictions for the ethylene glycol/paraffin results are less than half the rms differences of the measurements as a whole; therefore, the agreement between measurements and predictions is about as good as can be expected in view of experimental uncertainties.

Drop Deformation in Response to Shock-Wave Disturbances

The properties of drops subjected to shock-wave disturbances for a given initial diameter and gas-phase properties (specifically ρ_G and μ_G) are affected by the Weber number, the Ohnesorge number, the liquid/gas density ratio, the liquid/gas viscosity ratio, and the Reynolds number. (Note that the fifth parameter is a function of the other four; therefore, only four of these parameters are independent.) The effect of each of these variables on drop deformation and breakup will be considered in the following, using the present numerical simulations to develop the predictions.

The general behavior of drops exposed to a shock-wave disturbance is shown by the computed visualizations of the flow illustrated in Fig. 6. In this figure the shape of the liquid/gas interface is illustrated as a function of time for $Re = 50$, $\rho_L/\rho_G = 2$, $Oh = 0.01$, and $We = 2$, 8, and 32. In these figures the ambient flow is from left to right, the leftmost contour is the initial condition at $t/t^* = 0$ and $t/t^* = 1, 2, 3, \ldots, 6$ as the figures progress from left to right, where $t^* = (\rho_L/\rho_G)^{1/2} d_0/u_0$ is the characteristic drop breakup time proposed by Ranger and Nicholls.[26] These conditions correspond to the region between the onset of deformation observed during experiments of Hsiang and Faeth[1–3] and the onset of breakup observed during the experiments discussed by Hinze,[7] Hanson et al.,[27] Krzeczkowski,[28] Wierzba and Takayama,[29] and Gel'fand.[30] The main difference between the conditions of the experiments and predictions is that the experiments involved $\rho_L/\rho_G > 500$, whereas the predicted results illustrated in Fig. 6 were carried out for $\rho_L/\rho_G = 2$. It will be shown later, however, that the liquid/gas density ratio does not have a large effect on the deformation properties of liquid drops subjected to shock-wave disturbances; therefore, the results illustrated in Fig. 6 resemble the experimental results mentioned earlier. The liquid drop is seen to respond to the motion of the ambient gas by both translating in the streamwise direction and deforming from its initial circular shape. The translation is caused by the drag of the ambient flow on the liquid drop as a whole. The shape deformation comes about because acceleration of the ambient fluid over the liquid drop causes reduced pressures near the position of the maximum cross-stream (or frontal) area of the drop; this causes the liquid to move in the cross-stream direction until it is brought to a stop by surface tension forces. Increased Weber numbers can be interpreted as increased destabilizing drag force per unit stabilizing surface tension force; this causes a progressively larger cross-stream deformation of the drop leading to both larger drop drag coefficients and larger drop drag forces. The corresponding reduced liquid drop stability and increased drag force eventually leads to breakup of the liquid drop, based on the observations of Refs. 1–3, 5, and 27–30; however, breakup could not be specifically simulated during the present calculations because it involves the formation of nodes and other three-dimensional phenomena that cannot be treated because of the axisymmetric nature of the present numerical simulations. When liquid viscosity is small, as is the case for the results of Fig. 6 (e.g., $Oh = 0.01$) and for moderate levels of maximum deformation (e.g., $We = 2$ and 8 in Fig. 6), the drops reach a maximum deformation condition and then gradually return to a spherical shape in a decaying oscillatory manner because the acceleration of the drop eventually reduces the velocity difference between the drop and ambient fluid and thus the magnitude of the drag forces to a negligible value. Notably, similar oscillatory drop shape behavior was observed by Hsiang and Faeth[1] for $Oh < 0.1$ and $We > 2$ until drop

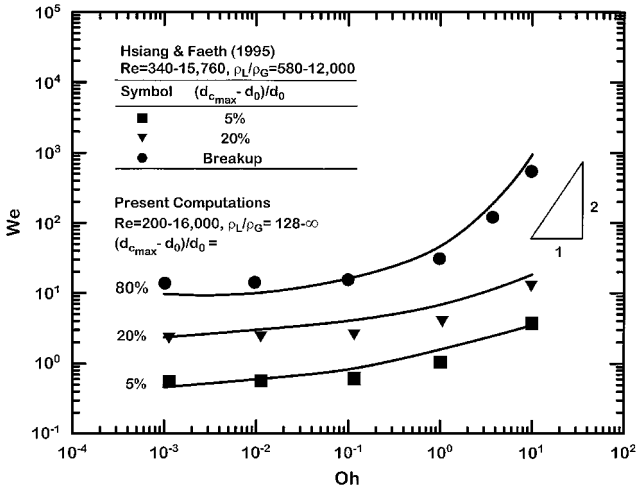

Fig. 7 Predicted and measured deformation and breakup regime map in the classical drop drag force/surface-tension-force (*We*) and liquid-viscous-force/surface-tension-force (*Oh*) coordinates of Hinze[7]: measurements from Hsiang and Faeth[3]; predictions from the present investigation.

breakup was observed, which is in qualitative agreement with the results illustrated in Fig. 6.

Measurements and numerical predictions of the maximum normalized deformation of drops, defined as $(d_{c\max} - d_0)/d_0$, subjected to shock-wave disturbances are illustrated in Fig. 7. This figure is plotted according to the classical Hinze[7] approach with deformation and breakup properties plotted as a function of the drop drag-force/surface-tension-force ratio (represented by the Weber number) and the drop liquid-viscous-force/surface-tension-force ratio (represented by the Ohnesorge number). The computations provide the normalized maximum drop deformation $(d_{c\max} - d_0)/d_0 = 5$, 20, and 80% as a function of Weber and Ohnesorge numbers. The computations were specifically carried out for liquid/gas density ratios of 128–∞ (reaching the infinite density ratio condition by extrapolation of the predictions which showed negligible effects of liquid/gas density ratio for values larger than 128) and for Reynolds numbers of the flow over the drop of 2×10^2–16×10^3. Measurements of drop deformation and breakup from Hsiang and Faeth[3] are also shown on the plots involving $(d_{c\max} - d_0)/d_0 = 5$ and 20% as well as their determination of the onset of breakup. These experiments involved $\rho_L/\rho_G = 580$–12,000 and $Re = 3.4 \times 10^2$–15.76×10^3; therefore, the conditions of the measurements and the predictions are comparable. The agreement between the measurements and the predictions is excellent. The results also show that a predicted normalized maximum deformation of 80% provides an excellent estimate of the conditions required for the onset of breakup. This predicted breakup approximation will be adopted in the following as a simplified way to estimate breakup using computations of deformation. As noted earlier, this approximation avoids the three-dimensional and high-resolution requirements of precise numerical simulations of breakup that would require excessive computational times and costs in order to consider the range of parameters treated during the current calculations, in view of current computer capabilities.

The classical Hinze[7] deformation and breakup regime plot was motivated by noting that when effects of liquid viscosity are small $Oh \ll 1$ drop stability implies that drop drag forces (proportional to $\rho_G u_0^2$) are balanced by drop surface-tension forces (proportional to σ/d_0), which implies that $\sigma/d_0 \sim \rho_G u_0^2$, or Ref. 7:

$$We_{\rm cr} = \left(\rho_G d_0 u_0^2 \big/ \sigma\right)_{\rm cr} = \text{constant}, \qquad Oh \ll 1 \qquad (4)$$

This approach is quite successful for correlating drop deformation and breakup properties when effects of liquid viscosity are small, yielding $We_{\rm cr} = \mathcal{O}(1)$ and $\mathcal{O}(10)$ for the onset of deformation and breakup, respectively, as indicated in Fig. 7. This approach has proven to be quite robust when liquid viscous effects are small because effects of liquid/gas density and viscosity ratios and Reynolds numbers are small for the range of conditions considered during typical experiments involving drop deformation and breakup caused by shock-wave disturbances, based on the results of the present computations, as noted earlier.

When surface tension effects become small, $Oh \gg 1$, drop stability implies that drop drag forces (proportional to $\rho_G u_0^2$) are balanced by drop liquid-viscous forces (proportional to $\mu_L u_{L0}/d_0 = \mu_L u_0 (\rho_G/\rho_L)^{1/2}/d_0$ after employing the Ranger and Nicholls[26] approximation for the characteristic liquid velocity, that is, $u_{L0} \sim (\rho_G/\rho_L)^{1/2} u_0$). In this case drop stability implies that $\mu_L (\rho_G/\rho_L)^{1/2} u_0/d_0 \sim \rho_G u_0^2$, or

$$We_{\rm cr} \sim \left[\mu_L^2 \big/ (\rho_L d_0 \sigma)\right]_{\rm cr} = Oh_{\rm cr}^2 = \text{constant}, \qquad Oh \gg 1 \qquad (5)$$

The tendency of the results illustrated to approach this behavior as Oh increases for values of Oh greater than unity is evident from the results illustrated in Fig. 7; the larger range of Oh of the deformation experiments of Hsiang and Faeth[1] provides additional evidence that the onset of particular degrees of deformation is represented by $We_{\rm cr} \sim Oh_{\rm cr}^2$ at large Ohnesorge numbers.

An undesirable feature of the classical Hinze[7] deformation and breakup regime map illustrated in Fig. 7 involves the awkward treatment of deformation and breakup regime transitions at large Ohnesorge numbers, where liquid viscosity is much more important for stabilizing drop deformation and breakup than the surface tension. In particular, the value of We at regime transitions varies with Oh at large Oh rather than remaining independent of Oh and providing a well defined value of We at the onset of various deformation and breakup transitions as at small Oh. A more convenient approach for representing conditions when effects of liquid viscosity are large, at large Ohnesorge-number conditions, can be obtained by accounting for liquid viscous effects directly by plotting drop deformation and breakup regime boundaries as functions of the ratio of drop drag forces (proportional to $\rho_G u_0^2$) to drop liquid-viscous forces [proportional to $\mu_L (\rho_G/\rho_L)^{1/2} u_0/d_0$], or

$$\text{drag forces/liquid-viscous forces} = We^{\frac{1}{2}} \big/ Oh \qquad (6)$$

as a function of the ratio of drop surface-tension forces to liquid viscous forces, or $1/Oh$. Figure 8 is an illustration of the drop deformation and breakup regime map in these new coordinates. Results illustrated in this figure are the same as those in Fig. 7; namely, computed maximum normalized drop deformations $(d_{c\max} - d_0)/d_0 = 5$, 20, and 80% from the present investigation and measured maximum normalized drop

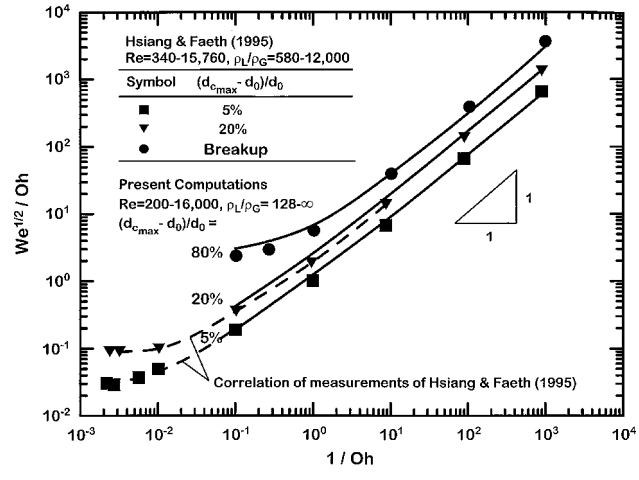

Fig. 8 Predicted and measured deformation and breakup regime map in the revised drop drag force/liquid-viscous-force ($We^{1/2}/Oh$) and surface-tension force/liquid-viscous-force ($1/Oh$) coordinates: measurements from Hsiang and Faeth[3]; predictions from the present investigation.

deformations $(d_{c\max} - d_0)/d_0 = 5$ and 20% and the corresponding drop breakup regime boundary, from Hsiang and Faeth[3]—the latter extending to values of Oh in the range 100–1000 that could not be reached at both large liquid/gas density ratios and large Reynolds numbers during present calculations because of increased computational costs at these conditions. As before, the comparison between predicted and measured deformations is very good, whereas the predicted 80% normalized deformation generally corresponds to the measured breakup regime boundary. The advantage of the deformation and breakup regime map of Fig. 8, however, is that the deformation and breakup regime boundaries are constant for $Oh \gg 1$. Naturally, when $Oh \ll 1$ and the deformation and breakup regime transitions are characterized by constant values of We, then $We^{1/2}/Oh \sim 1/Oh$ as indicated in Fig. 8. Finally, the tendency for regime transitions at large Ohnesorge numbers to be characterized by constant values of $We^{1/2}/Oh$ can be seen from the results illustrated in Fig. 8, particularly from the measurements of Hsiang and Faeth[3] that extend to relatively large values of Oh (or small values of $1/Oh$). Taken together, the deformation and breakup regime plots of Figs. 7 and 8 are complimentary: the classical Hinze[7] approach illustrated in Fig. 7 is particularly convenient when effects of liquid viscosity are small, whereas the modified approach illustrated in Fig. 8 is particularly convenient when effects of surface tension are small.

Computed Effects of Density Ratio and Reynolds Number on Deformation

Deformation and breakup regime maps in the new $We^{1/2}/Oh$ and $1/Oh$ coordinates were used to illustrate the effects of liquid/gas density ratio and Reynolds number on the deformation properties of drops subjected to shock-wave disturbances. Results for liquid/gas density ratio are plotted along these lines in Fig. 9. These results involve computations of the values of $We^{1/2}/Oh$ and $1/Oh$ required for a deformation $(d_{c\max} - d_0)/d_0 = 20\%$; for $\rho_L/\rho_G = 2$, 8, 32; and ∞ (the last by extrapolation) for a Reynolds number of the flow over the drop of 50. (Later results will show that effects of Reynolds number are relatively small for values of $Re \geq 50$.) The predictions show that effects of ρ_L/ρ_G for the very large range 2–∞ are relatively small for $1/Oh > 10$ (or $Oh < 0.1$). Even for values of $1/Oh < 10$, however, effects of ρ_L/ρ_G in the range 32–∞ remain relatively small (roughly 3:1) for large values of Oh. Because of the relationship between the onset of drop breakup and a critical degree of drop deformation for drops subjected to shock-wave disturbances, it is likely that effects of ρ_L/ρ_G variations on drop breakup properties are similar to those pictured for 20% deformation in Fig. 9; however, numerical simulations and experiments directly evaluating effects of liquid/gas density ratio on breakup clearly are merited.

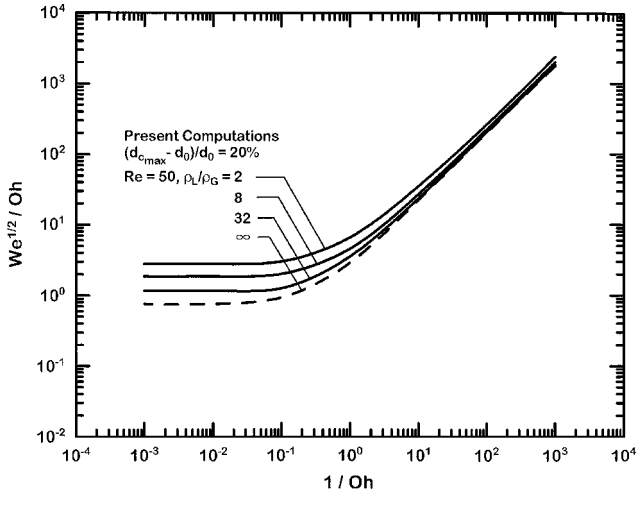

Fig. 9 Predicted effect of liquid/gas density ratio in the revised drop drag force/liquid-viscous-force ($We^{1/2}/Oh$) and surface-tension force/liquid-viscous-force ($1/Oh$) coordinates.

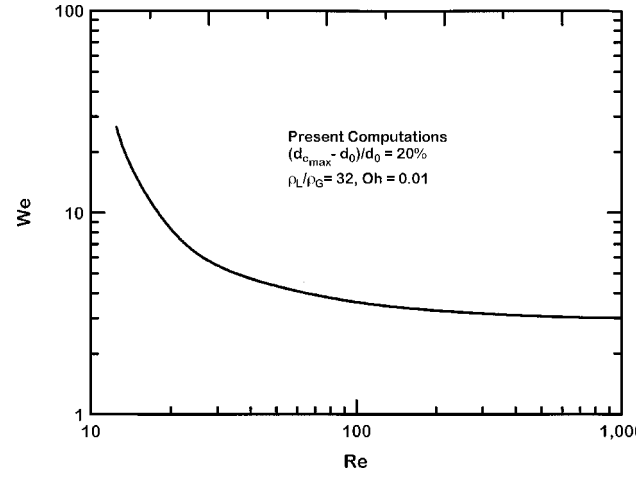

Fig. 10 Predicted effect of Reynolds number on drop deformation for $\rho_L/\rho_G = 32$ and $Oh = 0.01$.

Corresponding results considering effects of the initial Reynolds number of the flow over the drop on the deformation properties of drops subjected to shock-wave disturbances are illustrated in Fig. 10. These results involve the computation of the Weber number required for a maximum deformation, $(d_{c\max} - d_0)/d_0 = 20\%$, as a function of the Reynolds number of the flow over the drop for $\rho_L/\rho_G = 32$ and $Oh = 0.01$. As already noted, variations of ρ_L/ρ_G in the range 32–∞ have a relatively small effect on these results; corresponding variations of Oh, for $Oh < 1$, do not have a significant effect on these results as well. These predictions indicate that the Reynolds number has a relatively small effect on conditions required for particular levels of deformation for values in the range 100–1000 as already mentioned, for example, present predictions of mean drag coefficient are in good agreement with measurements in Fig. 3 in spite of effects of eddy shedding for $Re > 130$, whereas characteristic times of eddy shedding are small compared to drop relaxation time for present conditions so that the drops do not respond to effects of eddy shedding in any event. Reducing the Reynolds number to values below $Re = 100$, however, results in a substantial increase of the resistance of the drop to deformation, particularly when the Reynolds numbers become small as the creeping (Stokes) flow regime is approached. This behavior can be traced to the effect of Reynolds number on the drag coefficient of the drops (see Fig. 3). It is evident that the resistance of drops to deformation is correlated very strongly with the variation of the drop drag coefficient as a function of the Reynolds number. In particular, the weak variation of C_D with Reynolds number for $Re > 100$ corresponds to the relatively small effect of Reynolds number on drop deformation for these conditions, whereas the relatively large increase of C_D with Reynolds number for $Re \leq 100$ corresponds to the substantially increased resistance of drops to deformation in this region. These effects can be attributed to the more rapid relaxation of the drop velocity to the ambient velocity when C_D increases, which leaves less time for significant levels of deformation to develop before the relative velocity of the drop becomes small. Similar to the discussion of the effect of liquid/gas density ratio on the maximum drop deformation in connection with Fig. 3, however, direct experimental or numerical confirmation of effects of Reynolds number on the behavior of drop breakup clearly are needed.

Finally, the predictions were used to study the effect of liquid/gas density ratio on the dynamics of drop deformation caused by shock-wave disturbances. Some typical results of these computations are illustrated in Fig. 11, where the effect of the maximum deformation ratio $d_{c\max}/d_0$ on the normalized time to reach the maximum deformation condition $t_{\max}/t^*$ is plotted for various liquid/gas density ratios. When $\rho_L/\rho_G = 32$–∞ and $Re > 50$, the variation of $t_{\max}/t^*$ as a function of $d_{c\max}/d_0$ is universal—exhibiting little effect of variations of ρ_L/ρ_G and Reynolds number. For these conditions the results of the computations could be correlated

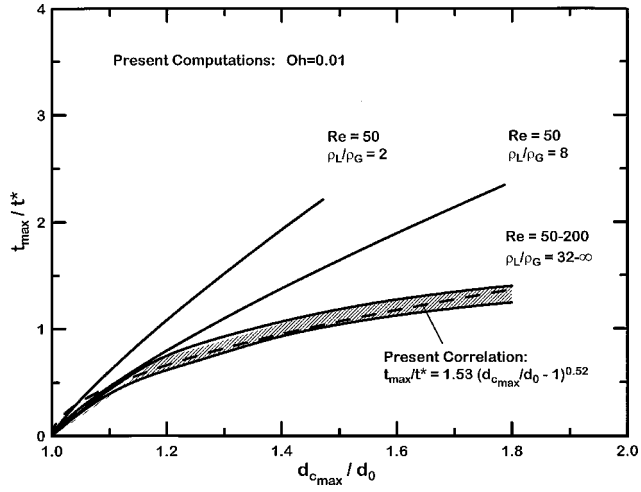

Fig. 11 Predicted normalized times to reach the maximum deformation condition t_{max}/t^*, as a function of the maximum deformation ratio $d_{c\,max}/d_0$.

as follows:

$$t_{max}/t^* = 1.53(d_{c\,max}/d_0 - 1)^{0.52}, \qquad \rho_L/\rho_G \geq 32, \qquad Re \geq 50 \tag{7}$$

Equation (4) indicates that effects of liquid/gas density ratio on drop deformation dynamics can be scaled reasonably well in terms of t/t^*, as suggested by Ranger and Nicholls[26] when ρ_L/ρ_G is large. For smaller values of ρ_L/ρ_G, however, reduction of ρ_L/ρ_G results in retarded development of drop deformation as a function of normalized time, in a region where t_{max}/t^* becomes a complex function of both the liquid/gas density ratio and the degree of deformation.

Conclusions

The major conclusions of the present computational study of the deformation, drag, and breakup properties of round liquid drops subjected to shock-wave disturbances are as follows:

1) Present predictions of the wake and drag properties of solid spheres and the deformation and breakup properties of deforming round liquid drops, subjected to steady and shock-wave disturbances, were in good agreement with existing measurements.

2) The liquid/gas density ratio had a surprisingly small effect on the deformation and breakup properties of drops subjected to shock-wave disturbances for values of $\rho_L/\rho_G > 32$, particularly when the Ohnesorge number is small.

3) The Reynolds number of the gaseous flow over the drop had a surprisingly small effect on the deformation and breakup properties of drops for $Re \geq 100$, where the drop drag coefficient is relatively independent of Reynolds number. However, as the Reynolds number was reduced and approached the Stokes range, drop resistance to deformation and breakup increased significantly because of the increase of the drag coefficient in this region. This allowed drops to approach gas velocities relatively rapidly and prevented them from reaching the relatively large deformations associated with drop breakup.

4) At large Ohnesorge numbers, surface tension has a negligible effect on drop deformation and breakup, which become more dominated by liquid viscous effects. This behavior introduces undesirable variations of the Weber number at drop deformation and breakup transitions as a function of the Ohnesorge numbers when plotted as functions of Weber and Ohnesorge numbers, as proposed by Hinze.[7] It was found that plotting the ratio of drop drag forces to liquid-viscous forces, $We^{1/2}/Oh$, as a function of the ratio of drop surface-tension forces to liquid-viscous forces, $1/Oh$, however, yielded deformation and breakup regime transitions that were relatively independent of Oh at large Ohnesorge numbers and provided a more convenient treatment of these transitions at conditions where effects of liquid viscosity dominate effects of surface tension for stabilizing drop deformation and breakup.

Acknowledgments

This research was sponsored by U.S. Air Force Office of Scientific Research Grants F49620-99-1-0083 and F49620-02-1-0007, under the technical management of J. M. Tishkoff.

References

[1]Hsiang, L.-P., and Faeth, G. M., "Near-Limit Drop Deformation and Secondary Breakup," *International Journal of Multiphase Flow*, Vol. 18, No. 5, 1992, pp. 635–652.

[2]Hsiang, L.-P., and Faeth, G. M., "Drop Properties After Secondary Breakup," *International Journal of Multiphase Flow*, Vol. 19, No. 5, 1993, pp. 721–735.

[3]Hsiang, L.-P., and Faeth, G. M., "Drop Deformation and Breakup due to Shock Wave and Steady Disturbances," *International Journal of Multiphase Flow*, Vol. 18, No. 4, 1995, pp. 545–560.

[4]Chou, W.-H., Hsiang, L.-P., and Faeth, G. M., "Temporal Properties of Drop Breakup in the Shear Breakup Regime," *International Journal of Multiphase Flow*, Vol. 23, No. 4, 1995, pp. 651–669.

[5]Chou, W.-H., Hsiang, L.-P., and Faeth, G. M., "Temporal Properties of Secondary Drop Breakup in the Bag Breakup Regime," *International Journal of Multiphase Flow*, Vol. 24, No. 6, 1995, pp. 889–912.

[6]Dai, Z., and Faeth, G. M., "Temporal Properties of Secondary Breakup in the Multimode Breakup Regime," *International Journal of Multiphase Flow*, Vol. 24, No. 6, 1998, pp. 889–912.

[7]Hinze, J. O., "Fundamentals of the Hydrodynamic Mechanism of Splitting in Dispersion Processes," *AIChE Journal*, Vol. 1, No. 3, 1955, pp. 289–295.

[8]Zaleski, S., Li, J., and Succi, S., "Two-Dimensional Navier–Stokes Simulation of Deformation and Breakup of Liquid Patches," *Physical Review Letters*, Vol. 75, No. 2, 1995, pp. 244–247.

[9]Han, J., and Tryggvason, G., "Secondary Breakup of Liquid Drops in Axisymmetric Geometry. I. Constant Acceleration," *Physics of Fluids*, Vol. 11, 1999, pp. 3650–3667.

[10]Han, J., and Tryggvason, G., "Secondary Breakup of Liquid Drops. II. Impulsive Acceleration," *Physics of Fluids*, Vol. 13, No. 6, 2001, pp. 1554–1565.

[11]Chorin, A. J., "Numerical Solution of the Navier–Stokes Equations," *Mathematics of Computations,* Vol. 22, No. 104, 1968, pp. 745–762.

[12]Harlow, F. H., and Welch, J. E., "Numerical Calculation of Time-Dependent Viscous Incompressible Flow of Fluid with Free Surface," *Physics of Fluids*, Vol. 8, No. 12, 1965, pp. 2182–2192.

[13]Sussman, M., Smereka, P., and Osher, J., "A Level Set Approach for Computing Solutions to Incompressible Two-Phase Flow," *Journal of Computational Physics*, Vol. 114, No. 1, 1994, pp. 146–159.

[14]Sussman, M., and Fatemi, E., "An Efficient Interface-Preserving Level Set Redistancing Algorithm and Its Application to Interfacial Incompressible Flow," *SIAM Journal of Scientific Computing*, Vol. 20, No. 4, 1999, pp. 1165–1191.

[15]Brackbill, J. U., Kothe, D. B., and Zemach, C., "A Continuum Method for Modeling Surface Tension," *Journal of Computational Physics*, Vol. 100, 1991, pp. 335–354.

[16]Taneda, S., "Experimental Investigation of the Wake Behind a Sphere at Low Reynolds Numbers," *Journal of the Physical Society of Japan*, Vol. 11, 1956, pp. 1104–1108.

[17]Pruppacher, H. R., LeClair, B. P., and Hamiliec, A. E., "Some Relations Between Drag and Flow Pattern of Viscous Flow past a Sphere and a Cylinder at Low and Intermediate Reynolds Numbers," *Journal of Fluid Mechanics*, Vol. 44, No. 4, 1970, pp. 781–790.

[18]Tomboulides, A., Orszag, S. A., and Karniadakis, G. E., "Direct and Large-Eddy Simulation of Axisymmetric Wakes," AIAA Paper 93-0546, 1993.

[19]Magnaudet, J., Rivero, M., and Fabre, J., "Accelerated Flows past a Rigid Sphere or a Spherical Bubble. Part 1. Steady Straining Flow," *Journal of Fluid Mechanics*, Vol. 284, 1995, pp. 97–135.

[20]Johnson, T. A., and Patel, V. C., "Flow past a Sphere up to a Reynolds Number of 300," *Journal of Fluid Mechanics*, Vol. 378, 1999, pp. 19–70.

[21]Roos, F. W., and Willmarth, W. W., "Some Experimental Results on Sphere and Disk Drag," *AIAA Journal*, Vol. 9, No. 2, 1971, pp. 285–291.

[22]LeClair, B. P., Hamiliec, A. E., and Pruppacher, H. R., "A Numerical Study of the Drag of a Sphere at Low and Intermediate Reynolds Numbers," *Journal of Atmospheric Science*, Vol. 27, No. 2, 1970, pp. 308–345.

[23]Dennis, S. C. R., and Walker, J. D. A., "Calculation of the Steady Flow past a Sphere at Low and Moderate Reynolds Numbers," *Journal of Fluid Mechanics*, Vol. 48, No. 4, 1971, pp. 771–789.

[24]Fornberg, B., "Steady Viscous Flow past a Sphere at High Reynolds Numbers," *Journal of Fluid Mechanics*, Vol. 190, 1988, pp. 471–489.

[25]Fadlun, E. A., Verzicco, R., and Mohd-Yusof, J., "Combined Immersed-Boundary Finite-Difference Methods for Three-Dimensional Complex Flow Simulations," *Journal of Computational Physics*, Vol. 161, No. 1, 2000, pp. 35–60.

[26]Ranger, A. A., and Nicholls, J. A., "The Aerodynamics and Shattering of Liquid Drops," *AIAA Journal*, Vol. 7, No. 2, 1969, pp. 285–290.

[27]Hanson, A. R., Domich, E. G., and Adams, H. S., "Shock-Tube Investigation of the Breakup of Drops by Air Blasts," *Physics of Fluids*, Vol. 6, No. 8, 1963, pp. 1070–1080.

[28]Krzeczkowski, S. A., "Measurement of Liquid Droplet Disintegration Mechanisms," *International Journal of Multiphase Flow*, Vol. 6, 1980, pp. 227–239.

[29]Wierzba, A., and Takayama, K., "Experimental Investigation of the Aerodynamic Breakup of Liquid Drops," *AIAA Journal*, Vol. 26, No. 11, 1988, pp. 1329–1335.

[30]Gel'fand, B. E., "Droplet Breakup Phenomena in Flows with Velocity Lag," *Progress in Energy and Combustion Science*, Vol. 22, 1996, pp. 201–265.

A. R. Karagozian
Associate Editor